$K\beta$ spectra of heliumlike iron from tokomak-fusion-test-reactor plasmas

A. J. Smith
Lock Haven University, Lock Haven, Pennsylvania 17745

M. Bitter, H. Hsuan, K. W. Hill, S. von Goeler, and J. Timberlake
Plasma Physics Laboratory, Princeton University, P.O. Box 451, Princeton, New Jersey 08543

P. Beiersdorfer and A. Osterheld
Lawrence Livermore National Laboratory, Livermore, California 94550
(Received 8 October 1992)

$K\beta$ spectra of heliumlike iron, Fe XXV, have been observed from tokamak-fusion-test-reactor (TFTR) plasmas with a high-resolution crystal spectrometer. The wavelength range of the Fe $K\beta$ spectrum partially overlaps the spectrum of heliumlike nickel (Ni XXVII), which is used on TFTR and the joint European torus for ion-temperature measurements. The experimental arrangement made it possible to observe the Fe XXV $K\beta$ lines and their satellite transitions of the type $1s2l'3l'' \rightarrow 1s^2 2l'$, as well as the entire satellite spectrum of the Ni XXVII $K\alpha$ line simultaneously. In order to identify the features of the $K\beta$ spectra and to study their possible interference with the Ni XXVII spectrum, the intensity of the $K\beta$ spectrum was enhanced by the injection of iron into the plasma. Accurate wavelengths and intensities have been obtained and compared with different theoretical calculations.

PACS number(s): 32.30.Rj, 52.70.La

I. INTRODUCTION

High-resolution satellite spectra of high-Z atoms are important for the diagnostics of tokamak plasmas and solar flares, and they are also of interest in testing atomic theories, which must include relativistic and quantum-electrodynamic effects. In the large tokamaks, such as the tokamak fusion test reactor (TFTR), the joint European torus (JET), the large Japanese tokamak (JT-60 U), and the French Tore Supra, where large-volume (>40 m^3) plasmas with peak electron temperatures ~ 5 keV are maintained for several seconds, hydrogenlike and heliumlike ions of high-Z atoms such as titanium, chromium, iron, and nickel are readily produced. Line radiation from these highly stripped ions is used for electron- and ion-temperature diagnostics as well as for determination of charge-state distributions and ion-transport coefficients. In particular, the resonance line of heliumlike nickel [1–4] is employed on TFTR, JET, and Tore Supra for Doppler broadening and Doppler-shift measurements in order to determine the central ion temperature as well as toroidal and poloidal plasma velocities.

In the case of TFTR and Tore Supra, which use stainless steel (~ 70 at. % Fe, ~ 20 at. % Cr, ~ 7 at. % Ni) walls and Inconel (~ 70 at. % Ni, ~ 15 at. % Cr, ~ 7 at. % Fe, ~ 2.5 at. % Ti) bellows protective cover plates, iron and nickel are simultaneously present as wall-derived impurities. Thus the possibility exists that the Fe XXV $K\beta$ spectrum and the Ni XXVII $K\alpha$ spectrum, which fall in the wavelength range from 1.57 to 1.62 Å, interfere with each other. It is therefore of considerable interest to determine whether a distortion of the Ni $K\alpha$ spectrum by the Fe $K\beta$ spectrum impairs the ion-temperature measurements. In this paper, we investigate the $K\beta$ spectrum of heliumlike iron. Such a study is also very important since experimental data on $K\beta$ spectra are scarce.

Under normal TFTR operating conditions prior to 1987, when the present data were collected, the nickel $K\alpha$ radiation was much more intense than the iron $K\beta$ radiation [5]. Iron was therefore injected into the plasma by a laser ablation technique in order to enhance the iron $K\beta$ emission relative to the nickel $K\alpha$ emission. Thus it was possible to extract the Fe $K\beta$ spectrum from the obtained composite spectrum and to clearly identify most of the theoretically predicted features.

The experimental wavelengths of the $K\beta$ lines and the associated satellite features were determined relative to the positions of nickel $K\alpha$ lines with an accuracy of ~ 0.1 mÅ. An important result of our experiments is that the $K\beta$ features are found to be well separated from the nickel $K\alpha$ resonance line, so that there is no interference with the central ion-temperature measurements. As an additional benefit, observation of the time history of the $K\beta$ radiation following the iron injection makes it possible to study the confinement of metal impurity ions in TFTR plasmas.

The paper is organized as follows. Section II presents theoretical data on the iron $K\beta$ satellite spectrum obtained from the Hebrew University–Lawrence Livermore Atomic Code (HULLAC) package. The experimental results and data analysis are described in Sec. III. Conclusions are given in Sec. IV.

II. THEORY

The spectrum of interest includes the $K\beta$ lines of heliumlike iron, corresponding to the transitions $1s^2\,{}^1S_0 - 1s3p\,{}^1P_1$ and $1s^2\,{}^1S_0 - 1s3p\,{}^3P_1$, and the associat-

ed lithiumlike and berylliumlike satellites due to the transitions $1s^2 2l$-$1s2l'3l''$ and $1s^2 2s2l'$-$1s2s2l'3l''$. These satellites can be formed (1) in the process of dielectronic recombination of heliumlike or lithiumlike ions, or (2) by collisional inner-shell excitation of lithiumlike and berylliumlike ions from their ground states. In the first process, a free electron is captured by a heliumlike *or* lithiumlike ion into the $n=3$ level:

$$1s^2+e^-\rightarrow 1s2l'3l'' , \tag{1}$$

or

$$1s^2 2s+e^-\rightarrow 1s2s2l'3l'' . \tag{2}$$

The resulting autoionizing states given in Eq. (1) can decay by two types of radiative-decay schemes:

$$1s2l'3l''\rightarrow 1s^2 3l , \tag{3}$$

or

$$1s2l'3l''\rightarrow 1s^2 2l . \tag{4}$$

The first type provides satellites to the heliumlike $K\alpha$ resonance line. These so-called unresolved $n=3$ satellites lie very close to the $K\alpha$ resonance line and have been investigated rather well [6]. Of interest for the present paper are the transitions of the second type, which give rise to $n=2$ satellites of the $K\beta$ lines. Because the plasma also contains lithiumlike ions, we expect to find satellite transitions from the dielectronic recombination of lithiumlike ions by radiative decay of the excited states, given in Eq. (2):

$$1s^2 2s+e^-\rightarrow 1s2s2l'3l''\rightarrow 1s^2 2s2l' . \tag{5}$$

The relevant transitions due to the second process of direct electron-impact excitation of inner-shell electrons from lithiumlike and berylliumlike charge states involve only the ground states of these ions:

$$1s^2 2s+e^-\rightarrow 1s2s3l+e^- \tag{6}$$

and

$$1s^2 2s^2+e^-\rightarrow 1s2s^2 3l+e^- , \tag{7}$$

since the so-called zero-density limit applies to the low electron densities of TFTR plasmas.

In the following, we discuss the line emissivities for ions from different charge states. The emissivities of the heliumlike $K\beta$ lines can be represented by

$$\epsilon_{\mathrm{He}}=N_e N_{\mathrm{He}} C , \tag{8}$$

where N_e and N_{He} are the electron and heliumlike ion densities, and C is an effective excitation rate coefficient that takes into account direct excitation and radiative cascades. These rate coefficients were obtained with the HULLAC set of atomic codes, which calculate wave functions, energy levels, and radiative transition rates by the relativistic, multiconfiguration parametric potential method with full configuration interaction [7]. The collisional excitation rates were calculated in the distorted-wave approximation; an efficient technique, which performs an angular factorization of both the direct and exchange contributions to excitation cross sections and interpolates the necessary radial integrals as a function of threshold energy [8], was used. The excitation-rate coefficients obtained from these calculations are given in Table I as a function of the electron temperature.

The emissivities of the so-called collisional satellite lines, which result from inner-shell electron-impact excitation of the lithiumlike and berylliumlike charge states, are given by

$$\epsilon_{\mathrm{CS}}=N_e N_{\mathrm{Li(Be)}} C \frac{A_r^{sf}}{\sum_{f'} A_r^{sf'}+\sum_{i'} A_a^{si'}} , \tag{9}$$

where $N_{\mathrm{Li(Be)}}$ is the density of the lithiumlike or berylliumlike charge state, A_r^{sf} is the radiative transition probability for the transition in question, and A_a^{si} is the autoionization probability to some final state i. The excitation-rate coefficients C for the lithiumlike and berylliumlike ions were obtained by the same methods as were the rate coefficients for the heliumlike ions, while the autoionization rates were obtained from a factorization-interpolation technique using a single consistent potential for the bound and continuum orbitals [9]. The excitation-rate coefficients and transition probabilities for Fe XXIV and Fe XXIII are also listed in Table I.

The emissivities of the lithiumlike dielectronic satellites of the $K\beta$ lines can be represented by

$$\epsilon_d=N_e N_{\mathrm{He}} F_1^*(T_e) F_2(s) , \tag{10}$$

where the factor

$$F_1^*(T_e)=\frac{1}{2}\left[\frac{2\pi h}{mkT_e}\right]^{3/2}\exp\left[-\frac{E_s}{kT_e}\right] \tag{11}$$

depends only on the electron temperature, and

$$F_2(s)=\frac{g_s}{g_i}\frac{A_r^{sf}A_a^{si}}{\sum_{i'} A_a^{si'}+\sum_{f'} A_r^{sf'}} \tag{12}$$

is the line strength. Here g_s and g_i are the statistical weights of the autoionizing states and the ground states, respectively, and E_s is the energy of the satellite level above that of the heliumlike ground state. The emissivities of the berylliumlike dielectronic satellite lines are given by an expression similar to (10), except that N_{He} is replaced by N_{Li}. The intensity factors $F_2(s)$ for the strong lithiumlike and berylliumlike dielectronic satellites, calculated with the HULLAC package, are listed in Tables II and III, respectively.

TABLE I. Excitation-rate coefficients for direct electron-impact excitation from the ground states of (a) Fe XXV, Fe XXIV, and (b) Fe XXIII at electron temperatures between 1.2 and 4.0 keV. Also listed are the autoionization probabilities A_a^{si}, the radiative transition probabilities A_r, and the branching ratios, defined as $\beta_r = A_r^{sf}/(\sum_f A_r^{sf} + \sum_i A_a^{si})$. The numbers in square brackets are powers of 10.

Charge state	Excited state	λ^{a}_{theor} (Å)	A_a (s^{-1})	A_a (s^{-1})	β_r	Excitation-rate coefficients for Fe XXV and Fe XXIV at different electron temperatures: 1.5 keV	2.0 keV	2.5 keV	3.0 keV	3.5 keV
Fe XXV	$[1s3p_{3/2}]_1$	1.5732	0	1.3985[14]	0.940	5.974[−15]	2.077[−14]	4.370[−14]	7.161[−14]	1.018[−13]
	$[1s3p_{1/2}]_1$	1.5751	0	1.0757[13]	0.546	1.807[−15]	5.635[−15]	1.080[−14]	1.633[−14]	2.163[−14]
	$[1s2s3p_{3/2}]_{3/2}$	1.5853	5.8017[12]	4.8657[13]	0.608	1.842[−15]	6.159[−15]	1.258[−14]	2.015[−14]	2.813[−14]
	$[1s2s3p_{1/2}]_{1/2}$	1.5864	5.0193[11]	6.1784[13]	0.813	1.060[−15]	3.596[−15]	7.436[−15]	1.293[−14]	1.693[−14]
	$[1s2p_{1/2}3s]_{3/2}$	1.5878	1.0177[12]	1.0134[13]	0.252	3.078[−16]	1.054[−15]	2.194[−15]	3.571[−15]	5.051[−15]
	$[1s2p_{1/2}3s]_{1/2}$	1.5886	2.9939[11]	4.1506[12]	0.309	6.324[−17]	2.128[−16]	4.373[−16]	7.039[−16]	9.866[−16]
Fe XXIV	$[1s2s3p_{3/2}]_{1/2}$	1.5912	1.3235[12]	6.9929[13]	0.813	1.178[−15]	3.979[−15]	8.202[−15]	1.324[−14]	1.860[−14]
	$[1s2s3p_{3/2}]_{3/2}$	1.5913	1.7645[12]	6.3381[13]	0.738	2.302[−15]	7.728[−15]	1.586[−14]	2.549[−14]	3.572[−14]
	$[1s2s3p_{1/2}]_{3/2}$	1.5924	6.5669[12]	1.6307[13]	0.786	1.376[−15]	4.310[−15]	8.337[−15]	1.274[−14]	1.706[−14]
	$[1s2s3p_{1/2}]_{1/2}$	1.5926	1.2161[11]	3.4637[13]	0.776	5.423[−16]	1.631[−15]	3.035[−15]	4.469[−15]	5.779[−15]

Charge state	Excited state	λ^{a}_{theor} (Å)	A_a (s^{-1})	A_r (s^{-1})	β_r	Excitation-rate coefficients for Fe XXIII at different electron temperatures: 1.2 keV	1.6 keV	2.0 keV	3.0 keV	4.0 keV
Fe XXIII	$[1s2s^23p_{3/2}]_1$	1.6053	6.9341[11]	1.2430[14]	0.852	1.67441[−15]	7.801[−15]	1.956[−14]	6.635[−14]	1.220[−13]

TABLE II. Intensity factors for the lithiumlike dielectronic satellite lines of the iron $K\beta$ lines: only lines with line factors larger than 1% of the strongest satellite are listed. Numbers in square brackets signify powers of 10.

Transitions	λ_{theor} (Å)	g_s	A_a (s^{-1})	β_r	$F_2(s)$ (s^{-1})
$[1s2s3p_{3/2}]_{3/2}$-$1s^22s$	1.5853	4	5.80[12]	0.608	1.41[13]
$[1s2p_{3/2}3p_{3/2}]_{3/2}$-$1s^22p_{3/2}$	1.5900	4	1.66[13]	0.100	6.64[12]
$[1s2p_{3/2}3p_{3/2}]_{5/2}$-$1s^22p_{3/2}$	1.5907	6	3.30[13]	0.048	9.50[12]
$[1s2p_{3/2}3p_{1/2}]_{3/2}$-$1s^22p_{3/2}$	1.5912	4	3.96[13]	0.050	7.92[12]
$[1s2s3p_{3/2}]_{1/2}$-$1s^22s$	1.5912	2	1.32[12]	0.813	2.15[12]
$[1s2s3p_{3/2}]_{3/2}$-$1s^22s$	1.5913	4	1.76[12]	0.738	5.20[12]
$[1s2p_{3/2}3p_{1/2}]_{3/2}$-$1s^22p_{1/2}$	1.5922	4	3.38[12]	0.157	2.12[12]
$[1s2s3p_{1/2}]_{3/2}$-$1s^22s$	1.5924	4	6.70[11]	0.786	2.10[12]
$[1s2p_{1/2}3p_{3/2}]_{3/2}$-$1s^22p_{3/2}$	1.5931	6	3.12[13]	0.663	1.24[14]
$[1s2p_{1/2}3p_{3/2}]_{3/2}$-$1s^22p_{1/2}$	1.5933	4	9.02[12]	0.523	1.88[13]
$[1s2p_{3/2}3p_{3/2}]_{3/2}$-$1s^22p_{3/2}$	1.5946	4	4.78[12]	0.419	8.01[12]
$[1s2p_{3/2}3p_{1/2}]_{5/2}$-$1s^22p_{3/2}$	1.5949	6	6.49[12]	0.305	1.19[13]
$[1s2p_{3/2}3p_{1/2}]_{3/2}$-$1s^22p_{3/2}$	1.5954	4	3.38[12]	0.362	4.89[12]
$[1s2s3d_{5/2}]_{3/2}$-$1s^22p_{1/2}$	1.5980	4	4.50[12]	0.230	4.14[12]
$[1s2s3d_{5/2}]_{5/2}$-$1s^22p_{3/2}$	1.6013	6	3.76[12]	0.122	2.75[12]
$[1s2s3s_{1/2}]_{1/2}$-$1s^22p_{1/2}$	1.6034	2	4.33[13]	0.052	4.50[12]
$[1s2s3s_{1/2}]_{1/2}$-$1s^22p_{3/2}$	1.6067	2	4.33[13]	0.054	4.68[12]

III. EXPERIMENTAL RESULTS

The spectra were obtained from five nearly identical ohmically heated TFTR discharges with the following parameters: The plasma current and the toroidal magnetic field were $I_p = 1.4$ MA and $B_T = 3.2$ T, and the plasma major and minor radii were $R = 2.48$ m and $a = 0.80$ m. These discharges were in steady-state conditions during the period from 1.5 to 4.5 s, and had a peak electron temperature of 2.7 keV and a peak electron density of 4.3×10^{13} cm^{-3}. Figure 1 shows the time evolution of the electron temperature T_e and electron density N_e for a TFTR discharge, which is typical of the discharges used in this experiment. The electron-temperature and density data were obtained from electron cyclotron measurements and laser interferometry. Iron was injected into the plasma at 2.7 s by a laser ablation technique. The injection led to a substantial increase (30%) of the total radiated power, but did not affect the central electron temperature and electron density; see Fig. 1.

TABLE III. Intensity factors for berylliumlike satellites of the iron $K\beta$ lines; only lines with $F_2(s) \geq 2.0 \times 10^{12}$ s^{-1} are included. Numbers in square brackets signify powers of 10.

Transitions	λ_{theor} (Å)	g_s	$A_a^{s\to 0}$ (s^{-1})	β_r	$F_2(s)$ (s^{-1})
$[1s2s2p_{3/2}]_3$-$[1s^22s2p_{3/2}]_2$	1.6023	7	1.16[13]	0.112	4.55[12]
$[1s2s2p_{3/2}3p_{3/2}]_2$-$[1s^22s2p_{3/2}]_2$	1.6027	5	2.11[13]	0.054	2.85[12]
$[1s2s2p_{1/2}3p_{3/2}]_2$-$[1s^22s2p_{1/2}]_1$	1.6047	5	1.09[13]	0.107	2.92[12]
$[1s2s2p_{3/2}3p_{3/2}]_3$-$[1s^22s2p_{3/2}]_2$	1.6052	7	1.84[13]	0.081	5.22[12]
$[1s2s2p_{3/2}3p_{3/2}]_0$-$[1s^22s2p_{3/2}]_1$	1.6057	1	1.43[13]	0.367	2.62[12]
$[1s2s2p_{3/2}3p_{3/2}]_2$-$[1s^22s2p_{3/2}]_1$	1.6071	5	1.56[13]	0.281	1.10[13]
$[1s2s2p_{3/2}3p_{1/2}]_2$-$[1s^22s2p_{3/2}]_1$	1.6082	5	2.99[13]	0.326	2.44[13]
$[1s2s2p_{3/2}3p_{3/2}]_2$-$[1s^22s2p_{1/2}]_1$	1.6095	5	1.81[13]	0.153	6.92[12]
$[1s2s2p_{3/2}3p_{3/2}]_1$-$[1s^22s2p_{3/2}]_2$	1.6101	3	8.76[12]	0.503	6.61[12]
$[1s2s2p_{1/2}3p_{3/2}]_1$-$[1s^22s2p_{1/2}]_0$	1.6102	3	2.53[13]	0.148	5.62[12]
$[1s2s2p_{3/2}3p_{1/2}]_2$-$[1s^22s2p_{1/2}]_1$	1.6106	5	3.38[12]	0.271	2.29[12]
$[1s2s2p_{1/2}3p_{3/2}]_3$-$[1s^22s2p_{3/2}]_2$	1.6108	7	3.08[13]	0.614	6.62[13]
$[1s2s2p_{1/2}3p_{3/2}]_1$-$[1s^22s2p_{1/2}]_1$	1.6110	3	2.53[13]	0.425	1.61[13]
$[1s2s2p_{1/2}3p_{3/2}]_2$-$[1s^22s2p_{1/2}]_1$	1.6115	5	5.72[12]	0.361	5.16[12]
$[1s2s^23d_{5/2}]_3$-$[1s^22s2p_{1/2}]_1$	1.6116	5	4.22[12]	0.445	4.69[12]
$[1s2s2p_{3/2}3p_{3/2}]_2$-$[1s^22s2p_{3/2}]_2$	1.6119	5	1.81[13]	0.459	2.08[13]
$[1s2s2p_{1/2}3p_{3/2}]_1$-$[1s^22s2p_{1/2}]_0$	1.6120	3	4.04[12]	0.602	3.65[12]
$[1s2s2p_{3/2}3p_{1/2}]_3$-$[1s^22s2p_{3/2}]_2$	1.6125	7	5.83[12]	0.442	9.02[12]
$[1s2s2p_{3/2}3p_{1/2}]_2$-$[1s^22s2p_{3/2}]_2$	1.6130	5	3.38[12]	0.311	2.63[12]
$[1s2s2p_{3/2}3p_{1/2}]_2$-$[1s^22s2p_{3/2}]_1$	1.6130	5	2.73[13]	0.039	2.66[12]

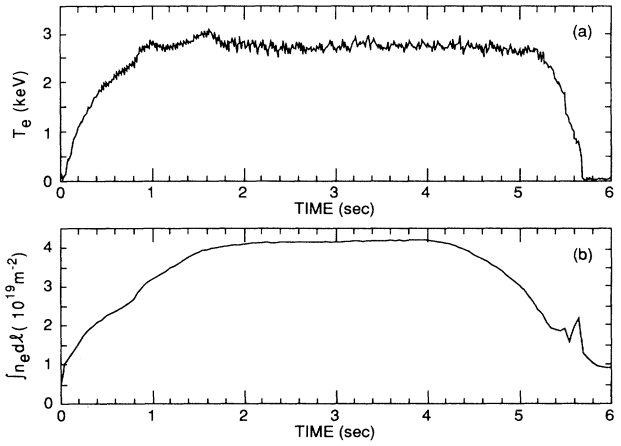

FIG. 1. Electron temperature and electron density as functions of time for a TFTR shot. The data were obtained from measurements of the electron cyclotron emission and laser interferometry. Iron was injected at 2.7 s by a laser ablation technique.

The spectral data were recorded with the TFTR horizontal and vertical curved crystal spectrometers [10,11]. The horizontal spectrometer was used to measure the composite spectra of the Ni XXVII $K\alpha$ and the Fe XXV $K\beta$ radiation. This spectrometer permits observation of spectral features in the wavelength range 1.57 to 1.62 Å, with a spectral resolving power of $\lambda/\Delta\lambda=7500$. The vertical spectrometer was used for simultaneous observation of the Fe XXV $K\alpha$ spectrum near 1.85 Å. Both spectrometers recorded 128 spectra from a discharge with a time resolution of 10 ms per spectrum, starting at 2.5 s.

Figure 2 shows the time history of the Fe XXV $K\alpha$ and $K\beta$ line intensities. These line intensities reach a maximum at 2.770 s, i.e., 70 ms after the injection of iron.

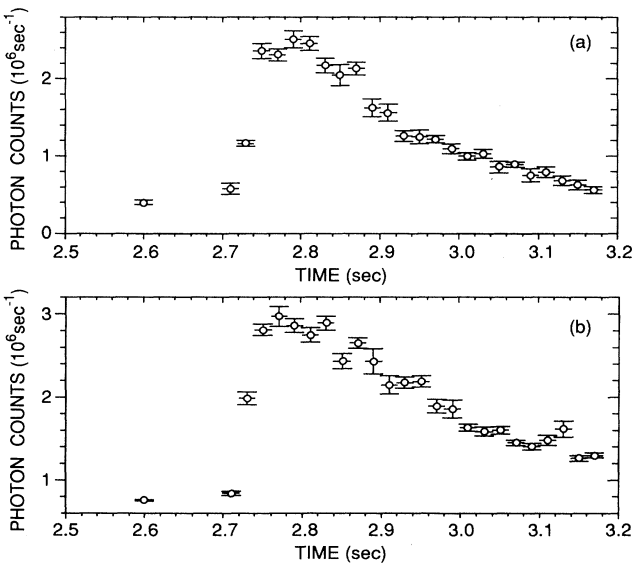

FIG. 2. Time history of (a) the Fe $K\beta$ and (b) the Fe $K\alpha$ line intensities.

The intensities then decay exponentially with an exponential-folding time of 300 ms, which is a measure of the particle-confinement time. A more detailed understanding of these data requires plasma-modeling calculations, e.g., with the multiion species transport (MIST) code [12], which takes into consideration the processes of ionization and recombination as well as ion transport due to diffusion and convection.

Figure 3 presents composite satellite spectra of the iron $K\beta$ and nickel $K\alpha$ lines from different time periods: (a) the period from 2.5 to 2.7 s before the injection of iron, and (b) the period from 2.75 to 2.88 s after injection, when the radiation from the injected iron is greater than 50% of its maximum value (see Fig. 2). The satellite spectrum of the Ni XXVII $K\alpha$ line has been described earlier by Hsuan *et al.* [1] and by Bitter *et al.* [4]. The dominant features of the Fe XXV $K\beta$ spectrum, the $1s^2\,{}^1S_0-1s3p\,{}^1P_1$ and $1s^2\,{}^1S_0-1s3p\,{}^3P_1$ transitions, are on the short-wavelength side of the Ni XXVII $K\alpha$ line between channels 140 and 160. It is evident from Figs. 3(a) and 3(b) that the iron $K\beta$ spectrum is very weak compared to the nickel spectrum under normal operating conditions in TFTR, but that it is enhanced by an order of magnitude following the iron injection. The second spectrum, Fig. 3(b), also shows some $K\beta$ satellite lines in the neighborhood of the nickel $K\alpha$ line w and in the wavelength range of the nickel features x and t; see Gabriel's notation [13]. These features are not apparent in Fig. 3(a). The nickel resonance line w, the dielectronic satellite line j, and the combined lines q and y, as well as β and z (see Gabriel's notation [13]) are not distorted by the iron lines, even during strong iron injection.

Since the electron temperature T_e and the electron density N_e were not affected by the iron injection, the

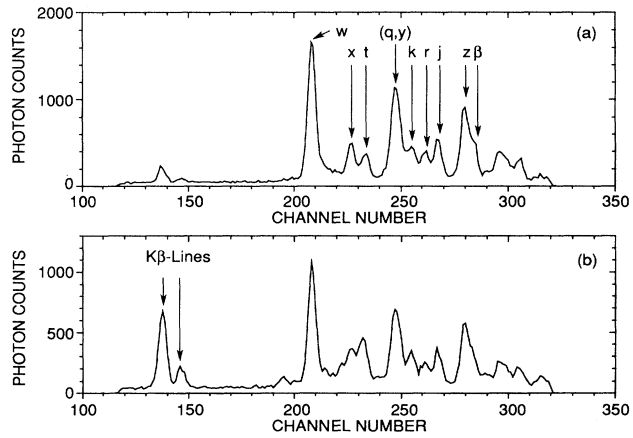

FIG. 3. Satellite spectra of Ni XXVII $K\alpha$ and Fe XXV $K\beta$ (a) before and (b) after iron injection. The data have been accumulated from five nearly identical TFTR ohmic shots during the periods (2.5–2.7) s for Fig. 3(a) and (2.75–2.88) s for Fig. 3(b). The features of the Ni XXVII $K\alpha$ satellite spectrum have been identified using Gabriel's notation [13]. The Fe XXV $K\beta$ features are significantly enhanced in the spectrum (b), which was recorded after iron injection.

TABLE IV. Experimental wavelengths and theoretical predictions for the lines in the iron $K\beta$ spectrum; peaks are numbered as in Fig. 4.

Peak	Transitions	Channel number	λ_{expt} (Å)	λ^{a}_{theor} (Å)	λ^{b}_{a} (Å)	λ^{c}_{b} (Å)	λ^{d}_{c} (Å)
1	$1s3p\ ^1P_1-1s^2\ ^1S_0$	137.85±0.07	1.57327±0.00003	1.5732	1.5732	1.57396	
2	$1s3p\ ^3P_1-1s^2\ ^1S_0$	146.47±0.17	1.57514±0.00005	1.5751	1.5751	1.57584	
3	$1s2s(^1S)3p\ ^2P_{3/2}-1s^22s\ ^2S_{1/2}$	194.70±0.12	1.58550±0.00004	1.5853	1.5855	1.58593	1.5858
4	$1s2s(^1S)3p\ ^2P_{1/2}-1s^22s\ ^2S_{1/2}$	200.75±0.22	1.58680±0.00005	1.5864	1.5866		1.5869
w[e]	$1s2p\ ^1P_1-1s^2\ ^1S_0$	208.27±0.05	1.5884		1.5884[f]		
5	$1s2s(^3S)3p\ ^2P_{1/2}-1s^22s\ ^2S_{3/2}$	222.42±0.13	1.59141±0.00004	1.5912	1.5915	1.59190	1.5917
	$1s2s(^3S)3p\ ^2P_{1/2}-1s^22s\ ^2S_{1/2}$			1.5913	1.5916	1.59190	1.5918
6	$1s2p(^3P)3p\ ^2D_{5/2}-1s^22p\ ^2P_{3/2}$	231.29±0.06	1.59330±0.00002	1.5931	1.5934	1.59387	1.5935
7	$1s2p(^3P)3p\ ^2P_{5/2}-1s^22p\ ^2P_{3/2}$	238.92±0.17	1.59491±0.00005	1.5949	1.5951	1.59567	1.5954
z[e]	$1s2s\ ^3S_1-1s^2\ ^1S_0$	279.87±0.12	1.60355±0.00003		1.6037		
8	$1s2s^23p\ ^1P_1-1s^22s^2\ ^1S_0$	289.41±0.59	1.60555±0.00012	1.6053	1.6055		
9	$1s2s2p3p\ ^3P_1-1s^22s2p\ ^3P_2$	315.70±0.57	1.61104±0.00012	1.6108			

[a] λ_{theor}: from our calculations.
[b] λ_a: See Ref. [14].
[c] λ_b: See Ref. [16].
[d] λ_c: See Ref. [15].
[e] Ni XXVII.
[f] Theoretical wavelength (Ref. [14]) used for normalization.

nickel spectrum of Fig. 3(a) can be normalized and subtracted from the composite nickel-iron spectrum of Fig. 3(b). The experimental iron $K\beta$ spectrum obtained in this way is shown in Fig. 4(a). The main features of the observed spectrum include the $K\beta$ lines (labeled 1 and 2) and the more prominent satellite transitions 3 through 9, which are identified in Table IV. In order to determine wavelengths of the observed spectrum accurately, the central channel numbers for the prominent peaks have been obtained by a least-squares fit of Voigt profiles to the experimental data. These central channel numbers, which are listed in Table IV with errors (ΔN) obtained from the least-squares-fitting procedure, have then been converted to wavelengths using the equation

$$\lambda = 2d \sin(\theta_0 + \Delta\theta) , \tag{13}$$

where $2d = 2.028$ Å is the $2d$ spacing of the quartz crystal (cut: $22\bar{4}3$) and $[\Delta\theta\ (\text{deg})] = 9.6880\times10^{-3}(N - N_0)$ is the dispersion of the instrument. N_0 and θ_0 are the channel number and the Bragg angle for the nickel line w. Since the spectrometer has no absolute wavelength calibration, the theoretical wavelength value of 1.5884 Å for the nickel w line from Vainshtein and Safronova [14] is used as a reference value, i.e., we assigned $\lambda_0^{theor} = 1.5884 = 2d \sin(\theta_0)$ to channel number N_0. The experimental wavelengths of the prominent features are shown in Table IV. The uncertainties of the experimental wavelengths given in Table IV have been determined from the uncertainties ΔN of the channel numbers using Eq. (13). The uncertainty of $\Delta N = 0.05$ for the position of the reference line w was also included in these calculations. We note that the experimental wavelengths have been determined relative to the Ni XXVII $K\alpha$ line with an

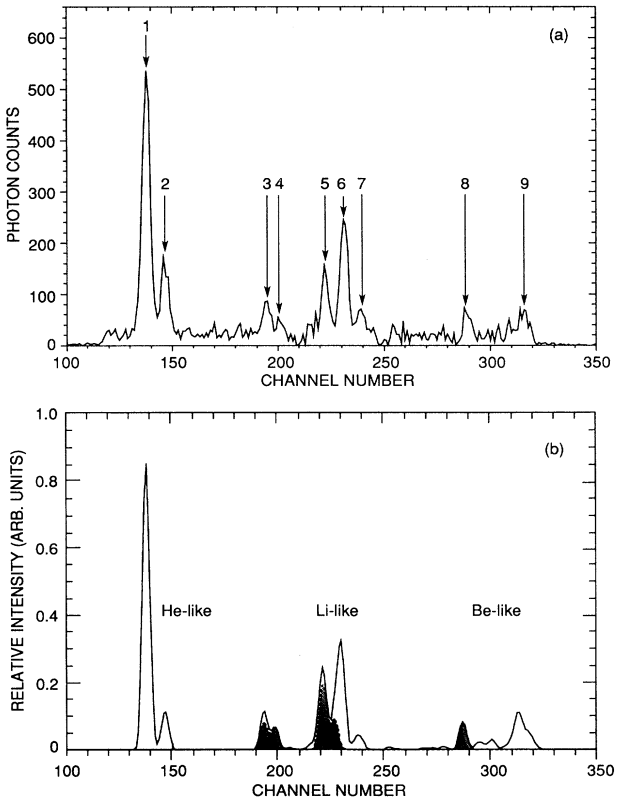

FIG. 4. (a) Experimental iron $K\beta$ spectrum obtained by subtracting a normalized spectrum of Fig. 3(a) from the spectrum shown in Fig. 3(b). (b) Synthetic iron $K\beta$ spectra constructed from present theoretical data for the measured electron and ion temperatures of $T_e = 2.7$ keV and $T_i = 2.35$ keV. The shaded area represents the satellite contributions from collisional inner-shell excitation. The solid line represents the entire spectrum including contributions from dielectronic recombination.

accuracy better than 0.1 mÅ. Also listed in Table IV are the theoretical wavelengths of the present calculations (see Tables II and III), and those from the calculations by Vainshtein and Safronova [14], Chen [15], and Nilsen [16]. Vainshtein and Safronova use the $1/Z$ expansion-perturbation technique, with relativistic corrections taken into account within the framework of the Breit operator. Chen [15] computes the relevant atomic data relativistically in intermediate coupling using configuration interaction in the multiconfiguration Dirac-Fock model (MCDF); a generalized Breit interaction and QED corrections were also taken into account. The third set of calculations, by Nilsen, uses MCDF for bound states and distorted-wave Dirac continuum states for electrons.

The different sets of theoretical wavelengths listed in Table IV are in good general agreement with the experimental wavelengths, given that these wavelengths can be shifted by a constant amount due to the fact that the spectrometer is not absolutely calibrated. The wavelengths of Vainshtein and Safronova seem to be more consistent with the observed data; the wavelengths from our calculations tend to be smaller than the observed values by about 0.3 mÅ, while those from Chen and Nilsen tend to be 0.2 and 0.7 mÅ, respectively, larger than the observed data.

Figure 4(b) shows a synthetic Fe XXV $K\beta$ spectrum constructed from the present theoretical data. The additional parameters, i.e., the electron and ion temperatures T_e and T_i, as well as the relative densities N_{He}, N_{Li}, and N_{Be} of the heliumlike, lithiumlike, and berylliumlike charge states of iron, have been derived from the iron $K\alpha$ spectrum, which was observed with the vertical TFTR spectrometer. The synthetic spectrum shown in Fig. 4(b) was obtained using $T_e = 2.7$ keV, $T_i = 3.0$ keV, and with N_{He}, N_{Li}, and N_{Be} in the ratio of 1.0:0.55:0.11.

IV. CONCLUSIONS

The Fe XXV $K\beta$ spectrum has been obtained from TFTR discharges and found to be in good agreement with a synthetic spectrum constructed from the present theoretical predictions. Since the iron $K\beta$ spectrum was partially blended with the Ni XXVII $K\alpha$ spectrum, it was necessary to enhance the intensity of the $K\beta$ radiation by the injection of iron into the plasma. A total of nine features in the Fe XXV $K\beta$ spectrum have been identified. The relative intensities depend on the electron temperature and charge-state balance, which suggests their future use for plasma diagnostics.

Experimental wavelengths of the Fe XXV $K\beta$ spectrum have been determined relative to the Ni XXVII $K\alpha$ resonance line with an accuracy better than 0.1 mÅ. The satellite lines of the iron $K\beta$ spectrum do not interfere with the Ni XXVII $K\alpha$ resonance line. This is important for both TFTR and Tore Supra plasmas, where iron and nickel are simultaneously present as impurities and where the Ni XXVII $K\alpha$ line is used for ion-temperature measurements.

ACKNOWLEDGMENTS

We deeply appreciate the fruitful discussions with Professor U. I. Safronova and would like to thank her for making her most recent wavelength calculations for the Fe XXV $K\beta$ spectrum available to us. We also gratefully acknowledge the continuing support of D. Meade, R. J. Hawryluk and K. M. Young, the technical assistance of J. Gorman, R. Such, and the TFTR operating crew, and software support by N. Schechtman. This work was supported by the U.S. Department of Energy, Contract No. DE-AC02-76-CHO-3073 and Contract No. W-7405-Eng-48.

[1] H. Hsuan, M. Bitter, K. W. Hill, S. von Goeler, B. Grek, D. Johnson, L. C. Johnson, S. Sesnic, C. P. Bhalla, K. B. Karim, F. Bely-Dubau, and P. Faucher, Phys. Rev. A **35**, 4280 (1987).

[2] F. Bombarda, R. Giannela, E. Källne, G. J. Tallents, F. Bely-Dubau, P. Faucher, M. Cornille, J. Dubau, and A. H. Gabriel, Phys. Rev. A **37**, 504 (1988); H. Hsuan, M. Bitter, J. E. Rice, K. W. Hill, L. Johnson, S. L. Liew, S. D. Scott, and S. von Goeler, Rev. Sci. Instrum. **59**, 2127 (1988).

[3] F. Bombarda, R. Giannella, E. Källne, and G. J. Tallents, J. Quant. Spectrosc. Radiat. Transfer **41**, 323 (1989).

[4] M. Bitter, H. Hsuan, V. Decaux, B. Grek, K. W. Hill, R. Hulse, L. A. Kruegel, D. Johnson, S. von Goeler, and M. Zarnstoff, Phys. Rev. A **44**, 1796 (1991).

[5] In 1987, the Inconel bellows cover plates were covered with graphite tiles, so that the concentration of nickel was very much reduced and iron became the dominant metal impurity in TFTR discharges. Line radiation from nickel could then no longer be used for ion-temperature measurements and the spectrometer was realigned for the observation of the Fe XXV $K\alpha$ line.

[6] F. Bely-Dubau, A. H. Gabriel, and S. Volonte, Mon. Not. R. Astron. Soc. **186**, 405 (1979); M. Bitter, S. von Goeler, K. W. Hill, R. Horton, D. Johnson, W. Roney, N. Sauthoff, E. Silver, and W. Stodiek, Phys. Rev. Lett. **47**, 921 (1981).

[7] M. Klapisch, Comput. Phys. Commun. **2**, 239 (1971); M. Klapisch, J. L. Schwob, B. S. Fraenkel, and J. Oreg, J. Opt. Soc. Am. **61**, 148 (1977).

[8] A. Bar-Shalom, M. Klapisch, and J. Oreg, Phys. Rev. A **38**, 1773 (1988).

[9] J. Oreg, A. Bar-Shalom, W. H. Goldstein, and M. Klapisch, Phys. Rev. A **44**, 1750 (1991).

[10] M. Bitter, K. W. Hill, S. Cohen, S. von Goeler, H. Hsuan, L. C. Johnson, R. Raftopoulos, M. Reale, N. Schechtman, F. Spinos, J. Timberlake, N. Young, and K. M. Young, Rev. Sci. Instrum. **57**, 2145 (1986).

[11] K. W. Hill, M. Bitter, M. Tavernier, M. Diesso, S. von Goeler, G. Johnson, L. C. Johnson, N. Sauthoff, N. Schechtman, S. Sesnic, F. Tenney, and K. M. Young, Rev. Sci. Instrum. **56**, 1165 (1985).

[12] R. A. Hulse, Nucl. Technol. Fusion **3**, 259 (1983).

[13] A. H. Gabriel, Mon. Not. R. Astron. Soc. **160**, 79 (1972).

[14] L. A. Vainshtein and U. I. Safronova [Acad. Sci. USSR], P. N. Lebedev Institute of Spectroscopy Report No. 2, 1985 (unpublished); U. I. Safronova (private communication).

[15] M. H. Chen, At. Data Nucl. Data Tables **34**, 301 (1986).

[16] J. Nilsen, At. Data Nucl. Data Tables **37**, 191 (1987).